Received: 10 April 2023 | Revised: 30 October 2023 | Accepted: 3 December 2023

DOI: 10.1002/1438-390X.12176

ORIGINAL ARTICLE

EDITOR'S CHOICE Population Ecology WILEY

Quantifying factors that explain the slopes of the temporal Taylor's law of Hokkaido vole populations

Takashi Saitoh[1] | **Joel E. Cohen**[2,3,4]

[1]Field Science Center, Hokkaido University, Sapporo, Japan

[2]Laboratory of Populations, The Rockefeller University, New York, New York, USA

[3]Earth Institute and Department of Statistics, Columbia University, New York, New York, USA

[4]Department of Statistics, University of Chicago, Chicago, Illinois, USA

Correspondence
Takashi Saitoh, Field Science Center, Hokkaido University,
Sapporo 060-0811, Japan.
Email: saitohtksh@gmail.com

Abstract

Taylor's law (TL) describes the relationship between the variance and mean of population density: $\log_{10}(\text{variance}) \approx \log_{10}(a) + b \times \log_{10}(\text{mean})$, $a > 0$. This study analyzed the temporal TL, for which mean and variance are calculated over time, separately for each population in a collection of populations, considering the effects of the parameters of the Gompertz model (a second-order autoregressive time-series model) and the skewness of the density frequency distribution. Time series of 162 populations of the gray-sided vole in Hokkaido, Japan, spanning 23–31 years, satisfied the temporal TL: $\log_{10}(\text{variance}_j) \approx 0.199 + 1.687 \times \log_{10}(\text{mean}_j)$. This model explained 62% of the variation of $\log_{10}(\text{variance}_j)$. An extended model with explanatory variables $\log_{10}(\text{mean}_j)$, the density-dependent coefficient for 1-year lag ($\alpha_{1,j}$), that for 2-year lag ($\alpha_{2,j}$), the density-independent variability (σ_j^2), and the skewness (γ_j), explained 93.9% of the $\log_{10}(\text{variance}_j)$ variation. In the extended model, the coefficient of $\log_{10}(\text{mean}_j)$ was 1.949, close to the null value ($b = 2$) of the TL slope. The standardized partial regression coefficients indicated that density-independent effects (σ_j^2 and γ_j) dominated density-dependent effects ($\alpha_{1,j}$ and $\alpha_{2,j}$) apart from $\log_{10}(\text{mean}_j)$. The negative correlations observed between σ_j^2 and $\log_{10}(\text{mean}_j)$, and between γ_j and $\log_{10}(\text{mean}_j)$, played an essential role in explaining the difference between the estimated slope of TL ($b = 1.687$) and the null slope ($b = 2$). The effects of those explanatory variables on $\log_{10}(\text{variance}_j)$ were interpreted based on the theory of a second-order autoregressive time-series model.

KEYWORDS

autoregressive time series, density dependence, density frequency distribution, slope, Taylor's law

1 | INTRODUCTION

Taylor's law (TL, Taylor, 1961) is an empirical rule describing the relationship between the variance and mean of population density in a set of populations. It has been verified in various ecological systems and many other fields (Taylor, 1986, 2019). TL asserts that the variance is approximately a power-law function of its mean: variance $\approx a \times (\text{mean})^b$, $a > 0$. It is often represented in the logarithmic form:

$$\log_{10}(\text{variance}) \approx \log_{10}(a) + b \times \log_{10}(\text{mean}). \quad (1)$$

The variance and mean of population density can be calculated temporally and spatially. In the temporal TL,

for each population separately, the variance and mean are calculated over observations of population density at different times. In the spatial TL, for each time separately, the variance and mean are calculated over observations of population density of spatially different populations. The temporal TL particularly gains interest in relation to population dynamics, and the slope b can be taken as a measure of the variation (from one population to another) in the magnitude of temporal population fluctuations as a function of the variation in the magnitude of the time-averaged population. The population-specific residuals in the temporal TL were proposed as a measure of stability in crop yields (Döring et al., 2015), and modified forms have been used to explore extinction risk in small-sized populations (Pertoldi et al., 2008; Reed & Hobbs, 2004). The temporal mean of population density may depend primarily on average habitat quality over time, while the temporal variance may depend on the internal dynamics of population fluctuation or environmental fluctuation over time or both, independently or in interaction. Therefore, analyses of the temporal variance–mean relationship may contribute to understanding not only the temporal TL but also population dynamics and population–environment interactions. This study investigated the temporal variance–mean relationship in relation to population dynamics.

Varied models (Ballantyne, 2005; Cohen, 2013; Kilpatrick & Ives, 2003) lead to a TL slope $b = 2$. However, most observed slopes satisfy $1 < b < 2$ (Cobain et al., 2019; Linnerud et al., 2013; Taylor & Woiwod, 1980, but see Zhao et al., 2019). These empirical slopes may be interpreted to suggest, in the temporal TL, that most populations fluctuate around a mean density as a result of regulatory forces inside or outside of the system in which the populations are involved, and the effect of forces may increase with rising mean density. Little evidence had accumulated by 1982 that the degree of density dispersion declined at high densities (Anderson et al., 1982). Reed and Hobbs (2004) demonstrated that the coefficient of variation (CV, equal to standard deviation divided by mean) became significantly weaker as the temporal mean population size increased in 2387 populations from 203 species. Although this negative relationship of density dispersion to mean density may reduce the slope compared to the null value of $b = 2$, an extended analysis, including other factors associated with the variance–mean ratio, should be carried out to assess the role of that negative relationship in TL. The relative importance of factors that affect the TL slope is poorly studied (Zhao et al., 2019), although many factors have been proposed as influential on TL slopes (e.g., species interaction: Kilpatrick & Ives, 2003, reproductive correlation: Ballantyne & Kerkhoff, 2007, habitat size: Mellin et al., 2010, demographic stochasticity: Linnerud et al., 2013, environmental variability: Cobain et al., 2019).

Cohen and Xu (2015) theoretically propose a baseline slope of TL based on their random sampling model, in which the TL slope is proportional to the skewness of the density frequency distribution when the mean and variance are constant. However, the baseline slope has not been fully utilized. Zhao et al. (2019) suggest population skewness, CV, and synchrony as useful analytical tools to understand how multiple ecological factors influence TL.

Although TL performs well describing the variance–mean relationship, the mean population density is not the only factor that may influence the variation of density variance. Cohen and Saitoh (2016) found that the density of 85 populations of the gray-sided vole, *Myodes rufocanus* (Sundevall, 1846), in Hokkaido satisfied the temporal TL (as well as a spatial TL) with $\log_{10}(\text{variance}) \approx 0.216 + 1.613 \times \log_{10}(\text{mean})$ with moderate goodness of fit ($R^2 = 0.607$). This motivated us to explore variables other than $\log_{10}$(mean) to explain the variation of $\log_{10}$(variance). Saitoh and Cohen (2018) suggested that the variance and mean of population density could be predicted from the density-dependent coefficients and density-independent parameters of the second-order autoregressive model based on Box and Jenkins (1970). Cohen and Xu (2015) showed mathematically that, assuming independent and identically distributed observations of population density, the TL slope could be predicted from the skewness and CV of population densities (see also Zhao et al., 2019). These theories tell us that the density-dependent coefficients, density-independent parameters, and the skewness of population density may help to explain the variation of $\log_{10}$(variance) besides $\log_{10}$(mean).

Here we report on the effects of mean densities, the density-dependent coefficients for 1-year and 2-year lags, the density-independent variability, and the skewness on the temporal variance of densities for 162 populations of the gray-sided vole. We show that the divergence of the empirical slope of the temporal TL from the null value ($b = 2$, which holds when the coefficient of variation is constant for different values of the temporal mean) can largely be explained by the interaction between mean densities and the density-independent variables. These results may contribute to understanding why most empirical temporal TL slopes are less than the null slope, $b = 2$.

2 | MATERIALS AND METHODS

2.1 | Study design and data

Hokkaido is the northernmost island of Japan (78,073 km^2). The gray-sided vole, *Myodes rufocanus* (Sundevall, 1846), is the commonest species of rodents on this island

(Kaneko et al., 1998), regarded as a pest species for forest plantations. The Japanese Government Forest Agency surveyed rodent abundance in natural forests for management purposes (Kaneko et al., 1998); the details of the rodent survey were described previously (Saitoh et al., 1997, 1998; Stenseth et al., 2003). The data analyzed in this study come from 162 gray-sided vole populations for which long time series (≥23 years) were accumulated in Hokkaido; 85 for 31 years (1962–1992), 19 for 27 years (1966–1992), and 58 for 23 years (1970–1992). Cohen and Saitoh (2016) and Saitoh and Cohen (2018) reported TL using a part of this data set: 85 time series spanning 31 years (1962–1992).

The 162 studied populations were widely distributed in the Hokkaido mainland (Figure 1). Saitoh et al. (1998) grouped those populations into seven groups according to geographic proximity and topographic characteristics. Populations in Group I and II were located in the Teshio and Kitami mountains, respectively; those in Group III were located in the Okhotsk area; those in Group IV were located in the Yubari mountains; those in Group V were located in the Kamikawa-Taisetsu mountains; those in Group VII were located in the west-side of the Hidaka mountains; and those in Group VIII were located in the mountainous parts of the Oshima peninsula. Some neighboring populations were grouped into different groups because the backbone of mountains or other topographic characteristics separated them. The populations of Group VI were not included in the analyses because their time series frequently recorded zeros. Two time series of Group VIII were excluded because their density-dependent coefficients (see Section 2.3) were not successfully estimated.

The warm sea current runs along the western coast of Hokkaido. The east coast is influenced by the cold sea current. The Okhotsk area has mixed influences from warm and cold sea currents. Therefore, the temperature of Hokkaido shows a decreasing gradient from southwest to northeast (Stenseth et al., 1998). The annual mean temperatures significantly varied among the study areas (Kruskal–Wallis rank sum test, $\chi^2 = 39.7$, $\mathrm{df} = 2$, $p = 2.4 \times 10^{-9}$, Figure S1): the southern areas for Group VIII, mean [range] = 8.2°C [6.8–9.7]; the western areas for Group I, IV, and VII, mean [range] = 5.8°C [4.5–7.5]; the eastern and inland areas for Group II, III, and V, mean [range] = 5.0°C [4.0–6.4]. These three areas had statistically significantly different temperatures (Dwass–Steel–Critchlow–Fligner test, $p < 1.0 \times 10^{-4}$).

Most natural forests of Hokkaido are classified as "pan mixed forest" with conifers and broad-leaved trees, whereas the Oshima peninsula, holding Group VIII, harbors temperate deciduous forests (Tatewaki, 1958). Conspicuous regional differences in mammalian fauna have not been reported.

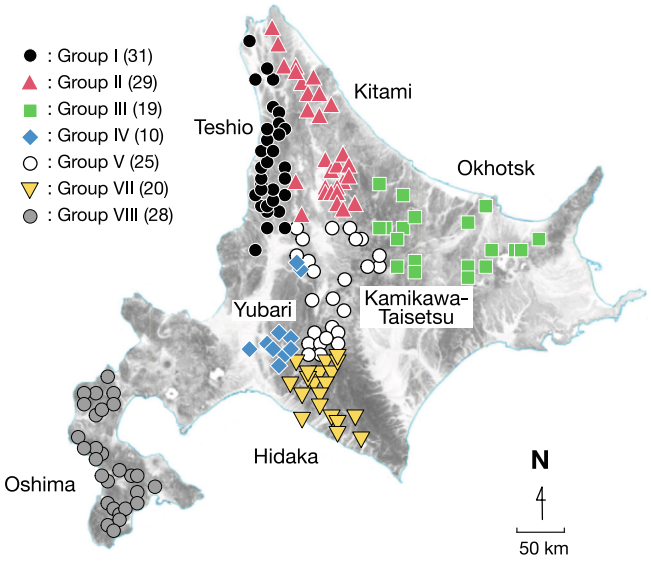

FIGURE 1 The map of the study area (the Hokkaido mainland). Mountain ridges illustrated by gray run north–south in the middle of the island, and the southwestern part (the Oshima peninsula) holds another mountain. The studied populations ($N = 162$), illustrated by different colored symbols, were grouped into seven groups according to geographic proximity and topographic characteristics by Saitoh et al. (1998). Populations in Group I and II are located in the Teshio and Kitami mountains; those in Group III are located in the Okhotsk area; those in Group IV are located in the Yubari mountains; those in Group V are located in the Kamikawa-Taisetsu mountains; those in Group VII are located in the west-side of the Hidaka mountains; those in Group VIII are located in the mountainous parts of the Oshima peninsula. Some neighboring populations were grouped into different groups because the backbone of mountains or other topographic characteristics separated them. Numbers in parentheses represent the number of populations for each group. [Correction added on 20 July 2024, after first online publication: The first five words in this sentence has been changed to "Numbers in parentheses represent" in this version.] The populations of Group VI were not included in the analyses because their time series frequently recorded zeros.

2.2 | Temporal Taylor's law

For each location j, the mean and variance were calculated over observations of population density ($N_{t,j}$) at different times t. The density estimation is described in the next section. One data point [$\log_{10}$(temporal mean$_j$), $\log_{10}$(temporal variance$_j$)] was plotted for each location j. Ordinary least-squares regression (OLS) was used to estimate the parameters of the temporal TL, by fitting Equation (1) to $\log_{10}$(temporal mean$_j$) and $\log_{10}$(temporal variance$_j$) of the vole populations. This method of estimating the parameters of the temporal TL implicitly assumes that the residuals (observed minus predicted values of the variance) from the linear relationship in Equation (1) are homoscedastic and independently distributed.

2.3 | Gompertz model

We used the Gompertz model, Equation (2), to describe the population dynamics of the gray-sided vole. In this model, for each population $j = 1$, ..., 162, $x_{t,j} = \ln(N_{t,j})$ was the natural logarithm of the empirically estimated density $N_{t,j}$ in year $t = 1962$, ..., 1992 (or 1966–1992, 1970–1992); μ_j was the temporal sample mean of $x_{t,j}$ in population j, and $X_{t,j} = x_{t,j} - \mu_j$ was the centered density on the natural logarithmic scale in population j. The Gompertz model supposes that

$$X_{t,j} = \left(1+\alpha_{1,j}\right) \times X_{t-1,j} + \alpha_{2,j} \times X_{t-2,j} + \text{Normal}\left(0, {\sigma_j}^2\right), \tag{2}$$

where for each population j, the parameters $\alpha_{1,j}$ and $\alpha_{2,j}$ are the coefficient of density dependence for a 1-year lag and for a 2-year lag, respectively. Although an autoregressive model can have an order higher than two (meaning that $X_{t,j}$ could depend on more than the two most recent prior values), most time series on microtine rodents have an order of approximately two (Stenseth, Bjørnstad, & Falck, 1996), and Stenseth, Bjornstad, and Saitoh (1996) confirmed that the second-order autoregressive model (Equation 2) was a parsimonious model for the studied populations. We used the Bayesian approach to estimate the densities and parameters under the assumption that $X_{t,j}$ came from a normal distribution with mean $= (1 + \alpha_{1,j})$ $X_{t-1,j} + \alpha_{2,j}X_{t-2,j}$ and variance$_j = {\sigma_j}^2$.

We linked the observation data (Vole$_{t,j}$: the number of voles captured at time t in location j) with the Gompertz model by assuming that Vole$_{t,j}$ is Poisson-distributed with mean shown in parenthesis on the right below:

$$\text{Vole}_{t,j} \sim \text{Poisson}\left(\text{Trap}_{t,j} \times \exp\left(\mu_j + X_{t,j}\right)\right),$$

where Trap$_{t,j}$ represents trapping effort (the number of trap-nights). Fitting the Gompertz model (Equation 2) to the centered time series $X_{t,j} = x_{t,j} - \mu_j$ yielded Bayesian estimates of $X_{t,j}$, $\alpha_{1,j}$, $\alpha_{2,j}$, μ_j, and σ_j. Population density ($N_{t,j}$) was defined as the number of voles captured per 150 trap-nights (50 snap traps for three consecutive nights on a 0.5 ha survey plot) and was obtained by multiplying $\exp(\mu_j + X_{t,j})$ by 150.

We programmed the model into RStan (Stan Development Team, 2022). The model parameters were estimated by 9000 iterations (after a 9000 iteration "burn in") under thin = 3 and chains = 4, although robust estimates were obtained under lower quantities of iterations and chains for most populations. This procedure was basically the same as in our previous works (Cohen & Saitoh, 2016; Saitoh, 2020; Saitoh & Cohen, 2018). We tested the validity of a gamma distribution (0.001, 0.001), which we used previously, for the non-informative prior distribution for σ_j, because Gelman (2006) suggested that a gamma distribution might cause a biased estimate for a very small σ_j and recommended instead a uniform distribution (0, 100). Using the 85 populations studied previously, which belonged to Groups I, II, and V in this study, we compared the parameter estimates between these two non-informative prior distributions. The gamma distribution provided consistently and slightly lower estimates compared to the uniform distribution (Figure S2). In most cases (>94%), the 95% credible intervals were smaller for parameter estimates from the gamma distribution than those from the uniform distribution. Therefore, we adopted estimates from the gamma distribution. The raw counts of voles trapped and the trapping effort (the number of trap-nights), the current Bayesian estimates of population densities, the locations of studied populations, and the program code using RStan are available in Supporting Information of this study.

2.4 | Theoretical predictions

We obtained theoretical predictions for the mean and variance of density of population j (on both the natural logarithmic and linear scales) from the population-specific density-dependent coefficients ($\alpha_{1,j}$ and $\alpha_{2,j}$) and density-independent parameter (${\sigma_j}^2$) of the Gompertz model (Box & Jenkins, 1970, pp. 58–63). Asymptotically for large time t, the variance ${z_j}^2$ of $X_{t,j}$ is, for every population j:

$${z_j}^2 = \frac{1-\alpha_{2,j}}{1+\alpha_{2,j}} \times \frac{\sigma_j^2}{\left(1-\alpha_{2,j}\right)^2 - \left(1+\alpha_{1,j}\right)^2}. \tag{3}$$

The formula in Equation (3) corrects a typographical error in the first displayed equation of appendix G of Saitoh and Cohen (2018), where *SD* should have an exponent 2. Population density on the linear scale ($N_{t,j}$) is, asymptotically for large time t, lognormally distributed with modeled mean, for every j,

$$E\left(N_{t,j}\right) = \exp\left(\mu_j + \frac{{z_j}^2}{2}\right) \tag{4}$$

and modeled variance, for every j,

$$\text{Var}\left(N_{t,j}\right) = \exp\left(2\mu_j + {z_j}^2\right) \times \left(\exp\left({z_j}^2\right) - 1\right). \tag{5}$$

From Equations (4) and (5), the relationship of Var($N_{t,j}$) to $E(N_{t,j})$ is, for every j:

$$\ln\left(\mathrm{Var}\left(N_{t,j}\right)\right)=2\times\ln\left(E\left(N_{t,j}\right)\right)+\ln\left(\left(\exp\left(z_j{}^2\right)-1\right)\right). \quad (6)$$

As $z_j{}^2$ becomes large, the ratio of $\exp\left(z_j{}^2\right)-1$ to $\exp\left(z_j{}^2\right)$ approaches 1, and then the ratio of $\ln\left(\exp\left(z_j{}^2\right)-1\right)$ to $\ln\left(\exp\left(z_j{}^2\right)\right)=z_j{}^2$ approaches 1. Further, the natural logarithm is converted to the logarithm with base 10, which is compatible with Equation (1):

$$\ln(10)\times\log_{10}\left(\mathrm{Var}\left(N_{t,j}\right)\right)=2\times\ln(10)\times\log_{10}\left(E\left(N_{t,j}\right)\right)+z_j{}^2.$$

Because $\ln(10)\approx 2.3$, the following relationship holds asymptotically for large z_j^2:

$$\log_{10}\left(\mathrm{Var}\left(N_{t,j}\right)\right)\sim 2\times\log_{10}\left(E\left(N_{t,j}\right)\right)+\frac{1}{2.3}\times z_j^2. \quad (7)$$

The skewness (γ) was defined following Cohen and Xu (2015):

$$\gamma\equiv\frac{m_3}{{m_2}^{3/2}},$$

where m_2 and m_3 are the second and third central moments, respectively (Table 1). The skewness (γ) was calculated using the package "e1071" 1.7-12 (Meyer et al., 2022) in the R statistical environment.

2.5 | Multiple linear regression analyses

Multiple linear regression analyses were carried out to identify factors influential on the variation of $\log_{10}(\mathrm{variance}_j)$ using $\log_{10}(\mathrm{mean}_j)$, the Gompertz model parameters $\alpha_{1,j}$, $\alpha_{2,j}$, and $\sigma_j{}^2$, and skewness of population densities (γ_j) as explanatory variables, considering the effects of the seven geographic groups. The analyses were extended to include all pairwise products of these five quantities ($\log_{10}(\mathrm{mean}_j)$, $\alpha_{1,j}$, $\alpha_{2,j}$, $\sigma_j{}^2$, and γ_j) as explanatory variables. Less influential explanatory variables were removed by the backward stepwise method using the stepAIC function in the package "MASS" of R, and the model with the smallest AIC was regarded as a best model. The multicollinearity among variables was tested using the variance inflation factor. Significant multicollinearity was not observed between individual variables (see Section 3). However, to minimize the effects of multicollinearity among products of explanatory variables, we centered all quantitative variables in models including multiplicative terms of quantitative explanatory variables. Variables were not centered in the models including multiplicative terms of quantitative and categorical (Group) explanatory variables.

All statistical analyses were carried out in R version 4.2.2 (R Core Team, 2022).

TABLE 1 A list of variables and parameters used in this study.

$\log_{10}(a)$: the intercept of the logarithmic form of the temporal TL, Equation (1)
b: the slope of the logarithmic form of the temporal TL, Equation (1)
$N_{t,j}$: an estimate of the density of population j in year t: $N_{t,j}=\exp(\mu_j+X_{t,j})\times 150$ (counts per 150 trap-nights)
$x_{t,j}$: the natural logarithm of $N_{t,j}$
μ_j: the sample temporal mean of the logarithmic density ($x_{t,j}$) for population j
$X_{t,j}$: the centered logarithmic density ($X_{t,j}=x_{t,j}-\mu_j$)
m_2: the second central moment (sum over t of $[N_{t,j}-\mathrm{mean}(N_{\cdot,j})]^2$, divided by number of years)
m_3: the third central moment (sum over t of $[N_{t,j}-\mathrm{mean}(N_{\cdot,j})]^3$, divided by number of years)
$\alpha_{1,j}$: the coefficient of density dependence for a 1-year lag for population j
$\alpha_{2,j}$: the coefficient of density dependence for a 2-year lag for population j
$\sigma_j{}^2$: the variance of the normal distribution of the error term for population j
γ_j: the skewness of the frequency distribution of densities in the natural scale for population j

3 | RESULTS

3.1 | Temporal Taylor's law

The temporal TL described the relationship of $\log_{10}(\mathrm{variance}_j)$ to $\log_{10}(\mathrm{mean}_j)$ of population density of the 162 observed populations moderately well (Figure 2, Model-0 using R notation for a linear model: $\log_{10}(\mathrm{variance}_j)\sim\log_{10}(\mathrm{mean}_j)$), with slope $b\pm$ standard error $=1.687\pm0.104$: $\log_{10}(\mathrm{variance}_j)=0.199$ ($\pm$ SE 0.084) $+1.687\times\log_{10}(\mathrm{mean}_j)$ (Adjusted $R^2=0.620$, Table S1). The lower and upper limits of the 95% confidence interval of slope estimate were 1.482 and 1.892, respectively. Quadratic regression revealed no statistically significant evidence of nonlinearity (Table S1).

The temporal TL was also supported by each seven geographic group with the following variations (see Table S1 for the detailed results):

$\log_{10}(\mathrm{variance}_j)=0.237+1.489\times\log_{10}(\mathrm{mean}_j)$ for Group I,

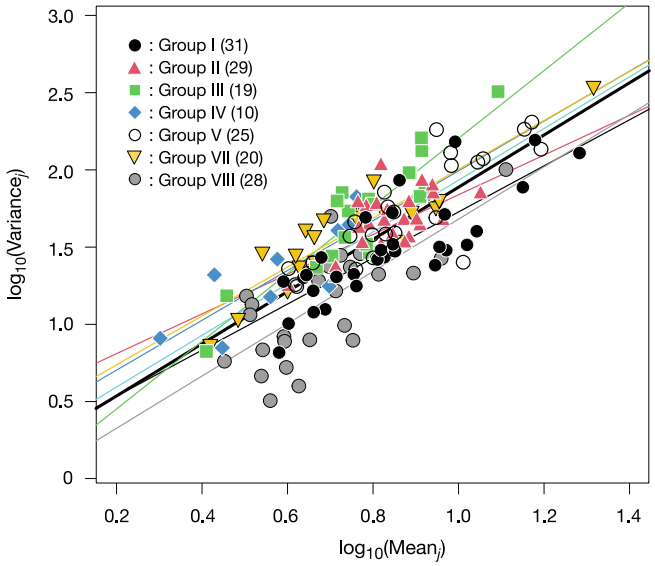

FIGURE 2 The temporal Taylor's law (TL): the relationship of $\log_{10}$(temporal variance$_j$) to $\log_{10}$(temporal mean$_j$) in 162 populations of the Hokkaido vole. Each population is plotted according to its variance and mean. The 162 populations are grouped into seven groups (Group I–V, VII, and VIII, see the study area map in Figure 1), illustrated by different symbols and colors (see the legend on the panel). The black bold line denotes the global temporal TL for all 162 populations: $\log_{10}(\text{variance}_j) = 0.199 + 1.687 \times \log_{10}(\text{mean}_j)$. The group-specific temporal TLs are illustrated by different colors corresponding to the symbol colors, except for Group V with light gray. The temporal TL showed the following variations: $\log_{10}(\text{variance}_j) = 0.237 + 1.489 \times \log_{10}(\text{mean}_j)$ for Group I, $\log_{10}(\text{variance}_j) = 0.554 + 1.284 \times \log_{10}(\text{mean}_j)$ for Group II, $\log_{10}(\text{variance}_j) = 0.015 + 2.187 \times \log_{10}(\text{mean}_j)$ for Group III, $\log_{10}(\text{variance}_j) = 0.382 + 1.610 \times \log_{10}(\text{mean}_j)$ for Group IV, $\log_{10}(\text{variance}_j) = 0.260 + 1.672 \times \log_{10}(\text{mean}_j)$ for Group V, $\log_{10}(\text{variance}_j) = 0.422 + 1.580 \times \log_{10}(\text{mean}_j)$ for Group VII, and $\log_{10}(\text{variance}_j) = -0.011 + 1.690 \times \log_{10}(\text{mean}_j)$ for Group VIII. The details of the TL analyses are available in Table S1.

$$\log_{10}(\text{variance}_j) = 0.554 + 1.284 \times \log_{10}(\text{mean}_j) \text{ for Group II,}$$
$$\log_{10}(\text{variance}_j) = 0.015 + 2.187 \times \log_{10}(\text{mean}_j) \text{ for Group III,}$$
$$\log_{10}(\text{variance}_j) = 0.382 + 1.610 \times \log_{10}(\text{mean}_j) \text{ for Group IV,}$$
$$\log_{10}(\text{variance}_j) = 0.260 + 1.672 \times \log_{10}(\text{mean}_j) \text{ for Group V,}$$
$$\log_{10}(\text{variance}_j) = 0.422 + 1.580 \times \log_{10}(\text{mean}_j) \text{ for Group VII, and}$$
$$\log_{10}(\text{variance}_j) = -0.011 + 1.690 \times \log_{10}(\text{mean}_j) \text{ for Group VIII.}$$

To test Group effects, Model-0 was modified to Model-1 ($\log_{10}(\text{variance}_j) \sim \log_{10}(\text{mean}_j) + \text{Group}$) and Model-2 ($\log_{10}(\text{variance}_j) \sim \log_{10}(\text{mean}_j) + \text{Group} + \log_{10}(\text{mean}_j) \times \text{Group}$). The comparison between Model-1 and Model-2 demonstrated no significant Group effect on the TL slopes (analysis of variance [ANOVA], $F = 0.911$, $p = 0.489$, Table S2), although the slope estimates varied from 1.284 to 2.187 and did not fall in the 95% CI of the slope (1.482–1.892) for overall populations. The comparison between Model-0 and Model-1 showed highly significant differences in the intercepts among Groups (ANOVA, $F = 15.082$, $p = 1.5 \times 10^{-13}$).

No significant nonlinearity was evident for any geographic group (Table S1).

3.2 | Population dynamics and density dependence

The vole counts per 150 trap-nights ranged from 0.05 to 73.26. The populations of Group II with the lowest TL slope exhibited an apparent oscillation with similar peak densities (Figure 3). In contrast, the peak densities of the Group III populations with the steepest TL slope greatly varied over the years. Population fluctuations of Group IV and VIII appeared milder than others. Their mean and variance of population densities were low, and their TL slopes were similarly moderate ($b = 1.610$ for Group IV and $b = 1.690$ for Group VIII). The relation of population dynamics patterns to the geographic location was unclear.

The synchrony of population dynamics, represented by the pairwise cross-correlation coefficient between population growth rates (Pearson's correlation coefficient, Bjørnstad et al. 1999) within a geographic group, varied significantly among the groups (Kruskal–Wallis rank sum test, $\chi^2 = 660.39$, df = 6, $p < 2 \times 10^{-16}$). It was highest in Group II with the lowest TL slope. Group III populations with the steepest TL slope showed similar population synchrony to Group II (Figure 3). The population synchrony was outstanding in eastern and inland populations in general. The mean population synchrony of the seven groups was not significantly associated with the group-specific temporal TL slopes (Pearson's correlation test, $r_p = 0.105$, $p = 0.823$).

The estimated mean of the density-dependent coefficient for 1-year lag ($\alpha_{1,j}$) ranged from −1.551 to 0.280 with mean = −0.826, while that for 2-year lag ($\alpha_{2,j}$) ranged from −0.767 to 0.580 with mean = −0.149 (Figure 4). These estimates extensively overlapped among the 162 populations, although $\alpha_{1,j}$ of Group VIII populations were higher than others. The mean of $\alpha_{1,j}$ was −0.376 for Group VIII populations, which was significantly higher than others (Figure 5, Kruskal–Wallis rank sum test, $\chi^2 = 69.278$, df = 6, $p = 5.8 \times 10^{-13}$). The mean of $\alpha_{1,j}$

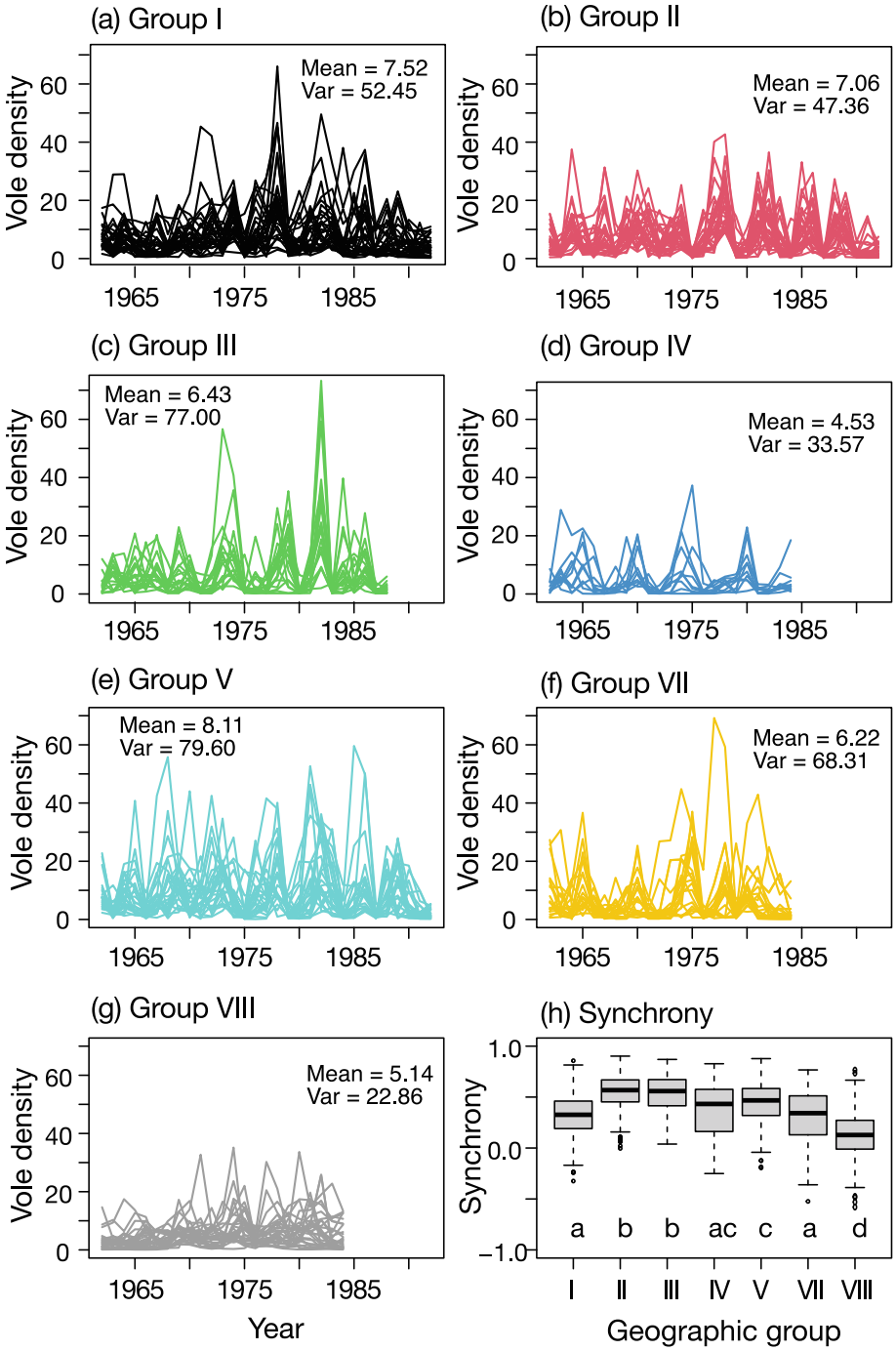

FIGURE 3 The population dynamics of the 162 studied populations. The populations are grouped into seven groups according to geographic proximity and topographic characteristics (see Figure 1). Population densities (counts per 150 trap-nights) in the linear scale are represented by a line for each population in each group. The length of time series varied between groups: 31 years for 31 populations of Group I (a), 29 populations of Group II (b), and 25 populations of Group V (e), 27 years for 19 populations of Group III (c), 23 years for 10 populations of Group IV (d), 20 populations of Group VII (f), 28 populations of Group VIII (g). The boxplot (h) indicates the synchrony of population dynamics, represented by the pairwise cross-correlation coefficient between population growth rates within a geographic group. The black lines in the boxes are the medians, and the box size is the interquartile range (IQR). The upper and lower whisker represents the maximum and minimum within 4 × IQR, respectively. The points outside of 4 × IQR are plotted as single points. Different letters denote a statistically significant difference between geographic groups (Kruskal–Wallis rank sum test and Dwass–Steel–Critchlow–Fligner test).

was close to −1 (−0.921), when excluding Group VIII populations. The upper limits of the 95% credible interval (95%CI) of $\alpha_{1,j}$ were lower than zero in 124 of 134 populations (92.5%) for six groups excluding Group VIII, while the significant populations for $\alpha_{1,j}$ were limited to seven out of 28 for Group VIII (25.0%, Figure S3).

The populations of Group I exhibited the largest variation of $\alpha_{2,j}$, covering the total range of this coefficient (Figure 4 and Figure 5). The mean of $\alpha_{2,j}$ for Group I was 0.045, which was significantly higher than others (Kruskal–Wallis rank sum test, $\chi^2 = 25.957$, $\mathrm{df} = 6$, $p = 0.0002$). Populations for which the upper limits of the 95% credible interval (95%CI) of $\alpha_{2,j}$ were lower than zero were restricted to 19 populations (11.7%, Figure S3). The Group II populations most frequently exhibited significant effects in $\alpha_{2,j}$ (38.1%), while no significant populations were found for $\alpha_{2,j}$ in Group III.

The parameter for density-independence (σ_j^2) also showed considerable variation among the seven groups (Figure 5, Kruskal–Wallis rank sum test, $\chi^2 = 73.004$, $\mathrm{df} = 6$, $p = 9.7 \times 10^{-14}$). Group VIII and Group III populations showed the lowest and highest σ_j^2, respectively.

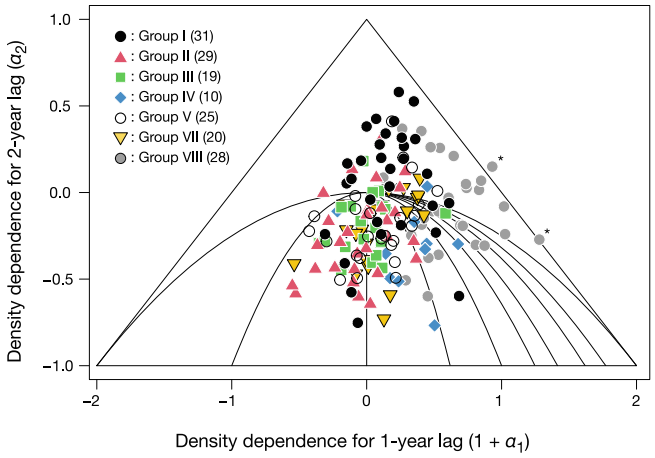

FIGURE 4 Density-dependent coefficients of the observed populations. The 162 populations are plotted according to the density-dependent coefficients based on the second-order autoregressive model (the Gompertz model). Inside the triangle, the dynamics is either point stability or damped fluctuations. The fluctuations will be persistent if any level of stochasticity is present. The dynamics is cyclic on the left side of $1 + \alpha_1 = 0$ or below the semicircle. The lines given are contours representing the periodicity in a continuous fashion inside the semicircle from the 3-year cycle (left-most) to 10-year cycle (right-most). Parameters outside the triangle lead to divergence (an unsustainable population). This figure is a modification of fig. 3.2 in Box and Jenkins (1970). The studied populations, illustrated by different colored symbols, were grouped into seven groups according to geographic proximity and topographic characteristics (see Figure 1). A figure in parentheses is the number of populations in each group. The variance of population densities predicted from Equation (5) was below zero for two populations denoted by asterisks.

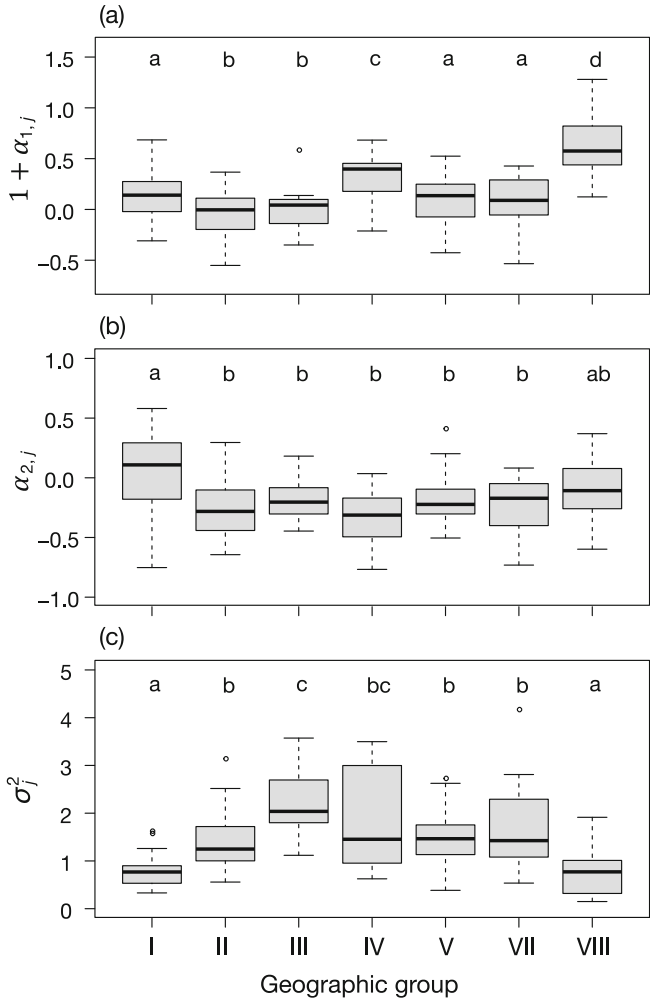

FIGURE 5 Boxplots for density-dependent coefficients ($\alpha_{1,j}$ and $\alpha_{2,j}$) and a density-independent parameter (σ_j^2) of the seven geographic groups based on a second-order autoregressive model (the Gompertz model). (a): density-dependent coefficients for 1-year lag ($1 + \alpha_{1,j}$), (b) density-dependent coefficients for 2-year lag ($\alpha_{2,j}$), and (c) a density-independent parameter (σ_j^2). The black lines in the boxes are the medians, and the box size is the interquartile range (IQR). The upper and lower whisker represents the maximum and minimum within 4 × IQR, respectively. The points outside of 4 × IQR are plotted as single points. Different letters denote a statistically significant difference among geographic groups (Kruskal–Wallis rank sum test and Dwass–Steel–Critchlow–Fligner test).

The group means of $\alpha_{1,j}$, $\alpha_{2,j}$ and σ_j^2 were not associated with the group-specific TL slopes ($r_p = 0.011$, $p = 0.981$ for $\alpha_{1,j}$, $r_p = -0.037$, $p = 0.938$ for $\alpha_{2,j}$, and $r_p = 0.542$, $p = 0.209$ for σ_j^2).

To assess the uncertainty of the model coefficients and parameter, the SEs of the estimates were examined. The SEs of $\alpha_{1,j}$ and $\alpha_{2,j}$ were highly correlated ($r_p = 0.936$, $p < 2 \times 10^{-16}$). The SEs of σ_j^2 showed significant but moderate associations to the SE of $\alpha_{1,j}$ and also to the SE of $\alpha_{2,j}$ ($r_p = 0.438$, $p = 5.3 \times 10^{-9}$ for the SE of $\alpha_{1,j}$ and $r_p = 0.375$, $p = 9.1 \times 10^{-7}$ for the SE of $\alpha_{2,j}$). Therefore, it may not be adequate to represent the uncertainty of the model coefficients and parameter by one index.

3.3 | Frequency distribution of population density

The densities $N_{t,j}$ on the linear scale from 162 populations ranged from 0.05 to 73.26 individuals per 150 trap-nights, with the mean = 6.774 and the skewness = 2.598. Smaller values were more frequent and very large values were rare (Figure 6a). The distribution was approximated by a negative-binomial distribution. The parameters of the negative binomial distribution were estimated by the method of moments, which gives the desired number of successes or shape parameter = 0.925 = mean^2/(variance − mean) and the probability of success = 0.120 = mean/variance. The Weibull distribution (shape = 1, scale = 7.5) also showed a good agreement with the frequency distribution. The median (4.32) was smaller than the mean.

The skewness for each population (γ_j) ranged from 0.087 to 3.834. The mean of local skewnesses γ_j, 1.499, was smaller than the overall skewness, 2.598. Although the density distribution was closer to the normal distribution on the natural logarithmic scale than the linear scale, it was skewed to the left (skewness = −0.439).

The density frequency distribution varied between the seven geographic groups (Figure 6b–h). Although the frequency in the smallest bin ($N_{t,j} < 1$) was the largest in five of the seven groups, the frequency in the second bin was the largest in Group I, and the frequencies in the first three bins were similar in Group VIII. The negative-binomial distribution appeared better to approximate the density frequency distribution for Group I and VIII than the Weibull distribution. In contrast, the Weibull distribution appeared better for Group II. The skewnesses of the seven geographic groups were not associated with the group means and variance of population densities ($r_p = -0.159$, $p = 0.733$ for mean density and $r_p = 0.288$, $p = 0.470$ for density variance). However, a significant correlation was detected between the group-specific skewness and the TL slope ($r_p = 0.775$, $p = 0.041$).

The log–log survival plot for population densities and the survival probabilities for the largest 10% of population densities (the 10% tail slope) were analyzed to assess the density frequency distribution further, following Cohen et al. (2022). The log–log survival plot was concave for overall populations (Figure S4). The Weibull survival curve fitted the empirical survival pattern well, while the empirical survival curve fell off faster than the lognormal survival curve.

The 10% tail slopes of the seven geographic groups become progressively more negative from the lowest to the highest mean density, including two exceptions (Figure S4): −2.436 (Group IV) > −3.622 (Group VIII) "<" −2.348 (Group VII) > −5.071 (Group III) > −7.041 (Group II) "<" −4.674 (Group I) > −7.501 (Group V). The 10% tail slopes and group density means were statistically significantly negatively correlated (Spearman's rank correlation test, $\rho = -0.786$, $p = 0.048$). These results indicate that the density distributions in these vole populations are not heavy-tailed, but are consistent with finite means, variances, and several finite higher moments. This behavior differed from the distributions of COVID-19 cases and deaths in United States counties, which satisfied a spatial TL and had a distribution with finite mean but infinite variance (Cohen et al., 2022).

3.4 | Variables explaining variation in the variance

The temporal variance of population densities on the linear scale ranged from 3.166 to 347.961 in the 162 populations, and the $\log_{10}(\text{variance}_j)$ variation was explained moderately well by $\log_{10}(\text{mean}_j)$ (the temporal TL, Figure 2). We explored here a more comprehensive model than the temporal TL to explain the $\log_{10}(\text{variance}_j)$ variation, carrying out multiple linear regression analyses using $\log_{10}(\text{variance}_j)$ as a response variable and $\log_{10}(\text{mean}_j)$, $\alpha_{1,j}$, $\alpha_{2,j}$, ${\sigma_j}^2$, and γ_j (skewness) as explanatory variables; Model-10: $\log_{10}(\text{variance}_j) \sim \log_{10}(\text{mean}_j) + \alpha_{1,j} + \alpha_{2,j} + {\sigma_j}^2 + \gamma_j$.

Model-10 explained a high proportion of the $\log_{10}(\text{variance}_j)$ variation (Adjusted $R^2 = 0.939$, Table 2). Increasing $\alpha_{2,j}$ significantly lowered $\log_{10}(\text{variance}_j)$, while other explanatory variables positively affected $\log_{10}(\text{variance}_j)$. The standardized partial regression coefficients demonstrated the prominent effect of $\log_{10}(\text{mean}_j)$ and the small effect of the density dependent coefficients ($\alpha_{1,j}$ and $\alpha_{2,j}$): $\log_{10}(\text{mean}_j)$: 0.912, $\alpha_{1,j}$: 0.031, $\alpha_{2,j}$: −0.099, ${\sigma_j}^2$: 0.350, and γ_j: 0.349. Although pairwise correlations between the explanatory variables were significant for two of ten pairs (Figure S5, the correlations between $\alpha_{1,j}$ and γ_j and between ${\sigma_j}^2$ and γ_j), multicollinearity between individual variables, tested by variance inflation factors, was not significant ($\log_{10}(\text{mean}_j)$: 1.113, $\alpha_{1,j}$: 1.188, $\alpha_{2,j}$: 1.075, ${\sigma_j}^2$: 1.168, γ_j: 1.179).

Considering the uncertainty of the estimates of the Gompertz model parameters, 1/(the averages of SEs for $\alpha_{1,j}$ and $\alpha_{2,j}$) were used as the weights in the multiple linear regression analysis. In a separate analysis, 1/(the SEs of ${\sigma_j}^2$) were used as the weights. These provided similar results to those of Model-10, but the model performance, assessed by R^2, was not improved by weighting (Table S3).

To test the effect of geographic groups, Model-10 was modified into Model-11 and Model-12.

$$\text{Model}-11:\ \log_{10}(\text{variance}_j) \sim \log_{10}(\text{mean}_j) + \alpha_{1,j} + \alpha_{2,j} + {\sigma_j}^2 + \gamma_j + \text{Group}.$$

$$\text{Model}-12:\ \log_{10}(\text{variance}_j) \sim \log_{10}(\text{mean}_j) + \alpha_{1,j} + \alpha_{2,j} + {\sigma_j}^2 + \gamma_j + \text{Group} + \text{Group} \times \log_{10}(\text{mean}_j) + \text{Group} \times \alpha_{1,j} + \text{Group} \times \alpha_{2,j} + \text{Group} \times {\sigma_j}^2 + \text{Group} \times \gamma_j.$$

The comparison between Model-10 and Model-11 demonstrated no significant Group effects on the intercepts (ANOVA, $F = 1.607$, $p = 0.149$, Table S4), while the comparison between Model-11 and Model-12 showed significant differences in the coefficients of the explanatory variables among Groups (ANOVA, $F = 2.588$, $p = 0.0001$).

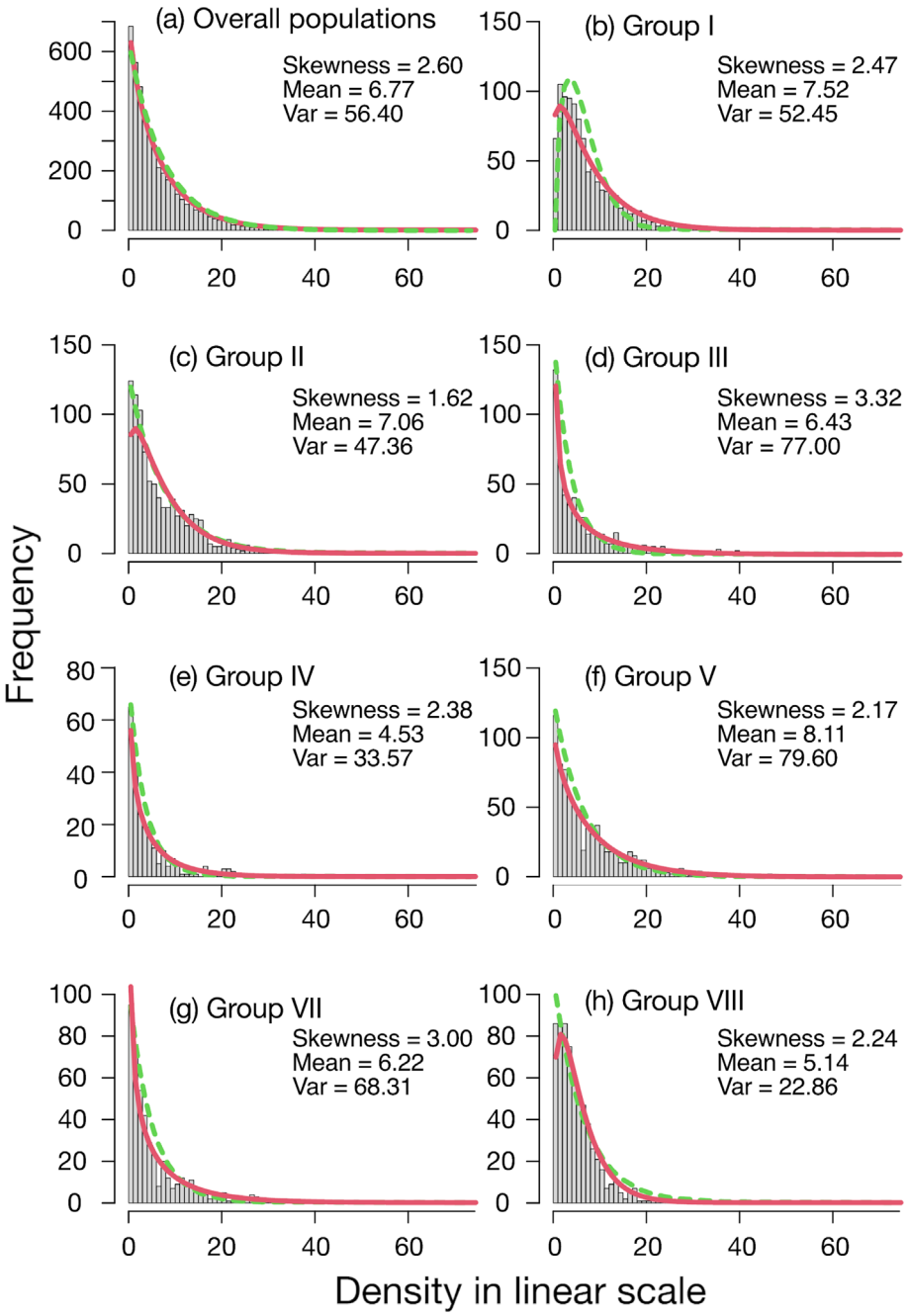

FIGURE 6 The frequency distribution of population densities in the linear scale. (a) Overall populations include 4482 densities from 162 populations. The distribution was well approximated by the negative binomial distribution with size = 0.925, the probability of success = 0.120 (the solid curve) and the Weibull distribution with shape = 1, scale = 7.5 (the dashed curve). (b) 31 populations for 31 years of Group I, approximated by the negative binomial distribution with size = 1.257, the probability of success = 0.143 (the solid curve) and the Weibull distribution with shape = 1.5, scale = 6.5 (the dashed curve). (c) 29 populations for 31 years of Group II, approximated by the negative binomial distribution with size = 1.236, the probability of success = 0.149 (the solid curve) and the Weibull distribution with shape = 1, scale = 7.5 (the dashed curve). (d) 19 populations for 27 years of Group III, approximated by the negative binomial distribution with size = 0.585, the probability of success = 0.083 (the solid curve) and the Weibull distribution with shape = 1, scale = 3.75 (the dashed curve). (e) 10 populations for 23 years of Group IV, approximated by the negative binomial distribution with size = 0.707, the probability of success = 0.135 (the solid curve) and the Weibull distribution with shape = 1, scale = 3.5 (the dashed curve). (f) 25 populations for 31 years of Group V, approximated by the negative binomial distribution with size = 0.919, the probability of success = 0.102 (the solid curve) and the Weibull distribution with shape = 1, scale = 6.5 (the dashed curve). (g) 20 populations for 23 years of Group VII, approximated by the negative binomial distribution with size = 0.623, the probability of success = 0.091 (the solid curve) and the Weibull distribution with shape = 1, scale = 4.9 (the dashed curve). (h) 28 populations for 23 years of Group VIII, approximated by the negative binomial distribution with size = 1.491, the probability of success = 0.225 (the solid curve) and the Weibull distribution with shape = 1, scale = 6.5 (the dashed curve).

TABLE 2 The results of the multiple linear regression analysis using the model for $\log_{10}(\text{variance}_j)$ with five independent explanatory variables.

Model-10: $\log_{10}(\text{variance}_j) \sim \log_{10}(\text{mean}_j) + \alpha_{1,j} + \alpha_{2,j} + \sigma_j^2 + \gamma_j$.

Coefficients	Estimate	SE	*t*-value	*p*
(Intercept)	−0.529	0.045	−11.648	$<2 \times 10^{-16}$
$\log_{10}(\text{mean}_j)$	1.949	0.044	44.560	$<2 \times 10^{-16}$
$\alpha_{1,j}$	0.036	0.024	1.468	0.144
$\alpha_{2,j}$	−0.138	0.028	−4.946	1.9×10^{-6}
σ_j^2	0.166	0.010	16.719	$<2 \times 10^{-16}$
γ_j	0.182	0.011	16.592	$<2 \times 10^{-16}$

Note: Regression coefficient estimates (Estimate), standard error (SE), *t* value, and *p*-value for *t*-test are given. See Table 1 for the details of explanatory variables. Residual standard error: 0.093 on 156 degrees of freedom. Multiple R^2: 0.941, Adjusted R^2: 0.939. *F*-statistic: 500.5 on 5 and 156 df, *p*-value: $<2 \times 10^{-16}$.

The model was further extended to include all explanatory variables and pairwise products of the five quantities using centered variables (sometimes called "multiplicative terms").

$$\begin{aligned}\text{Model}-13:\ &\log_{10}(\text{variance}_j) \sim \log_{10}(\text{mean}_j) + \alpha_{1,j} + \alpha_{2,j} \\ &+ \sigma_j^2 + \gamma_j + \log_{10}(\text{mean}_j) \times \alpha_{1,j} \\ &+ \log_{10}(\text{mean}_j) \times \alpha_{2,j} + \log_{10}(\text{mean}_j) \\ &\times \sigma_j^2 + \log_{10}(\text{mean}_j) \times \gamma_j + \alpha_{1,j} \times \alpha_{2,j} \\ &+ \alpha_{1,j} \times \sigma_j^2 + \alpha_{1,j} \times \gamma_j + \alpha_{2,j} \times \sigma_j^2 + \alpha_{2,j} \\ &\times \gamma_j + \sigma_j^2 \times \gamma_j.\end{aligned}$$

To test the effect of geographic groups, Model-13 was compared to the following two models, Model-14 and Model-15.

$$\begin{aligned}\text{Model}-14:\ &\log_{10}(\text{variance}_j) \sim \log_{10}(\text{mean}_j) + \alpha_{1,j} \\ &+ \alpha_{2,j} + \sigma_j^2 + \gamma_j + \text{Group} + \log_{10}(\text{mean}_j) \\ &\times \alpha_{1,j} + \log_{10}(\text{mean}_j) \times \alpha_{2,j} + \log_{10}(\text{mean}_j) \\ &\times \sigma_j^2 + \log_{10}(\text{mean}_j) \times \gamma_j + \alpha_{1,j} \times \alpha_{2,j} + \alpha_{1,j} \\ &\times \sigma_j^2 + \alpha_{1,j} \times \gamma_j + \alpha_{2,j} \times \sigma_j^2 + \alpha_{2,j} \times \gamma_j + \sigma_j^2 \times \gamma_j.\end{aligned}$$

$$\begin{aligned}\text{Model}-15:\ &\log_{10}(\text{variance}_j) \sim \log_{10}(\text{mean}_j) + \alpha_{1,j} \\ &+ \alpha_{2,j} + \sigma_j^2 + \gamma_j + \log_{10}(\text{mean}_j) \times \alpha_{1,j} \\ &+ \log_{10}(\text{mean}_j) \times \alpha_{2,j} + \log_{10}(\text{mean}_j) \\ &\times \sigma_j^2 + \log_{10}(\text{mean}_j) \times \gamma_j + \alpha_{1,j} \times \alpha_{2,j} + \alpha_{1,j} \\ &\times \sigma_j^2 + \alpha_{1,j} \times \gamma_j + \alpha_{2,j} \times \sigma_j^2 + \alpha_{2,j} \times \gamma_j + \sigma_j^2 \\ &\times \gamma_j + \text{Group} + \text{Group} \times \log_{10}(\text{mean}_j) \\ &+ \text{Group} \times \alpha_{1,j} + \text{Group} \times \alpha_{2,j} + \text{Group} \\ &\times \sigma_j^2 + \text{Group} \times \gamma_j.\end{aligned}$$

Model-13 explained a high proportion of the $\log_{10}(\text{variance}_j)$ variation, and Adjusted R^2 slightly increased from 0.939 of Model-10 to 0.942 (Table S5). All independent explanatory variables ($\log_{10}(\text{mean}_j)$, $\alpha_{1,j}$, $\alpha_{2,j}$, σ_j^2, and γ_j) showed significant effects, but the only significant multiplicative term was $\sigma_j^2 \times \gamma_j$ among the 11 multiplicative terms. The comparison between Model-14 and Model-15 demonstrated significant differences in the coefficients of the explanatory variables among Groups (ANOVA, $F = 2.607$, $p = 0.0002$), while the comparison between Model-13 and Model-14 showed no significant Group effects on the intercepts (ANOVA, $F = 1.403$, $p = 0.217$).

Since the Group effects on the coefficients of the explanatory variables were not negligible, Model-13 was fitted separately to the overall populations and the populations of the seven geographic groups, and the best model with the smallest AIC was selected by the function of stepAIC. In the model selection for overall populations, ΔAIC was lower than two in 43 models. Five independent variables ($\log_{10}(\text{mean}_j)$, $\alpha_{1,j}$, $\alpha_{2,j}$, σ_j^2, and γ_j) were involved in all ten models with the smallest ten AIC (Table S6). The product of $\sigma_j^2 \times \gamma_j$ was retained in all models, while other multiplicative terms occurred intermittently. The best model consisted of the five independent variables and the four multiplicative terms ($\log_{10}(\text{mean}_j) \times \alpha_{1,j}$, $\log_{10}(\text{mean}_j) \times \alpha_{2,j}$, $\alpha_{2,j} \times \gamma_j$, and $\sigma_j^2 \times \gamma_j$).

The model selection showed consistent results on independent variables in the seven geographic groups; all five variables ($\log_{10}(\text{mean}_j)$, $\alpha_{1,j}$, $\alpha_{2,j}$, σ_j^2, and γ_j) were involved in all but one of the selected models; $\alpha_{1,j}$ was removed in Group II (Table 3). In contrast, the selection of multiplicative terms was inconsistent among the seven groups. Eight products ($\log_{10}(\text{mean}_j) \times \alpha_{1,j}$, $\log_{10}(\text{mean}_j) \times \alpha_{2,j}$, $\log_{10}(\text{mean}_j) \times \sigma_j^2$, $\alpha_{1,j} \times \alpha_{2,j}$, $\alpha_{1,j} \times \sigma_j^2$, $\alpha_{2,j} \times \sigma_j^2$, $\alpha_{2,j} \times \gamma_j$, and $\sigma_j^2 \times \gamma_j$) were included in the selected models of some but not all groups. Five of the seven selected models included $\log_{10}(\text{mean}_j) \times \alpha_{1,j}$, and four models included $\alpha_{1,j} \times \alpha_{2,j}$, $\alpha_{2,j} \times \sigma_j^2$, and $\sigma_j^2 \times \gamma_j$. Other multiplicative terms were found in fewer than four

TABLE 3 The models describing the variation of the variance of population density in logarithm with base 10.

Group	Intercept	m	α_1	α_2	σ^2	γ	$m \times \alpha_1$	$m \times \alpha_2$	$m \times \sigma^2$	$\alpha_1 \times \alpha_2$	$\alpha_1 \times \sigma^2$	$\alpha_2 \times \sigma^2$	$\alpha_2 \times \gamma$	$\sigma^2 \times \gamma$
All 162	0.011	1.957	0.056	−0.150	0.172	0.181	0.251	−0.271	NA	NA	NA	NA	−0.069	−0.046
Group I	0.009	1.677	0.117	−0.087	0.202	0.208	−0.526	0.587	NA	0.326	NA	NA	NA	NA
Group II	0.004	1.779	NA	−0.275	0.132	0.111	0.486	NA	0.574	NA	NA	−0.182	−0.316	NA
Group III	0.222	3.648	2.030	−0.394	−0.005	0.375	3.338	NA	−0.704	4.723	−1.695	0.733	0.279	−0.230
Group IV	−0.124	1.224	0.624	−0.420	0.1806	0.231	3.795	NA	NA	NA	NA	NA	NA	−0.164
Group V	0.049	1.946	0.152	−0.028	0.100	0.293	NA	NA	0.362	NA	NA	0.294	0.433	−0.160
Group VII	0.117	1.756	0.049	−0.470	0.167	0.099	2.349	−2.599	NA	−1.300	0.309	−0.655	NA	−0.076
Group VIII	−0.045	2.007	0.277	0.334	0.347	0.124	NA	NA	NA	−1.029	NA	NA	NA	NA

Note: The best model was selected for the 162 populations and each group by the backward stepwise method using stepAIC from Model-13 ($\log_{10}(\text{variance}) \sim \log_{10}(\text{mean}) + \alpha_1 + \alpha_2 + \sigma^2 + \gamma + \log_{10}(\text{mean}) \times \alpha_1 + \log_{10}(\text{mean}) \times \alpha_2 + \log_{10}(\text{mean}) \times \sigma^2 + \log_{10}(\text{mean}) \times \gamma + \alpha_1 \times \alpha_2 + \alpha_1 \times \sigma^2 + \alpha_1 \times \gamma + \alpha_2 \times \sigma^2 + \alpha_2 \times \gamma + \sigma^2 \times \gamma$). All variables were centered. "All 162" and "m" denote all 162 populations including all populations from Group I to VIII (excluding Group VI) and the mean of population density in logarithm with base 10, respectively; see Table 1 for other explanatory variables. Each explanatory variable (column heading) is given a coefficient when included in the model; NA = "not applicable" when an explanatory variable is omitted from the selected best model.

selected models. Therefore, we considered Model-10 with the five independent variables without multiplicative terms (Table 2) most consistent to explain the variation in $\log_{10}(\text{variance}_j)$.

All effects of $\log_{10}(\text{mean}_j)$, ${\sigma_j}^2$, and γ_j, which were highly significant in explaining variance_j, were positive in Model-10 (Table 2). To realize $b < 2$, the increase of $\log_{10}(\text{variance}_j)$ should slow as $\log_{10}(\text{mean}_j)$ increases. Thus, negative relationships between ${\sigma_j}^2$ and $\log_{10}(\text{mean}_j)$ and between γ_j and $\log_{10}(\text{mean}_j)$ were expected and observed (Pearson's correlation test, ${\sigma_j}^2$-$\log_{10}(\text{mean}_j)$: $r_p = -0.148$; γ_j-$\log_{10}(\text{mean}_j)$: $r_p = -0.157$, Figure S5).

3.5 | Test of theoretical predictions

The mean and variance of population density in each local population j were predicted from the density-dependent coefficients ($\alpha_{1,j}$ and $\alpha_{2,j}$) and density-independent parameter (${\sigma_j}^2$) (Equations 3–5). The mean densities were predicted within the realistic range from 0.00009 to 43.1 on the linear scale, in comparison with the observed range (2.2–20.8). In contrast, the predicted variance unrealistically widely ranged from −1.6 to 7.5×10^6 on the linear scale, while the observed range was between 3.1 and 348.0. The predicted variances of two populations of Group VIII were below 0 (namely, the two populations outside the triangle in Figure 4), and those of six populations (two of Group III, three of Group VII, and one population of Group VIII) exceeded 10,000. When excluding these unrealistic predicted variances, the predicted variances and means from the remaining 154 populations satisfied the temporal TL ($\log_{10}(\text{Var}(N_{t,j})) = 0.351\ (\pm\ \text{SE}\ 0.182) + 2.224\ (\pm\text{SE}\ 0.195) \times \log_{10}(E(N_{t,j}))$, $R^2 = 0.457$, and the 95% confidence interval of the slope 2.224 was 1.838–2.610 (Figure 7a). The slope was significantly steeper for the predicted values than for the observed ones (Table S6) because of the high predicted variances (Figure 7d).

The predicted variances of $\log(N_{t,j})$, which are necessary to predict the mean and variance of population densities from the Gompertz model parameters (${z_j}^2$, Equation 3), showed a clear relationship to the observed ones ([observed variance of $\log(N_{t,j})] = 0.146 + 0.627 \times {z_j}^2$, $R^2 = 0.880$, Figure 7b, and the 95% confidence interval of the slope 0.627 was 0.590–0.664), although ${z_j}^2$ were consistently higher than the observed variances. A similar pattern was observed in the relationship between the predicted and observed means; most predicted means were higher than the observed means ([observed $\text{mean}_j] = 0.964 + 0.640 \times$ [predicted mean_j], $R^2 = 0.587$, Figure 7c, and the 95% confidence interval of the slope 0.640 was 0.554–0.725). In contrast, on the linear scale (Figure 7d), the predicted

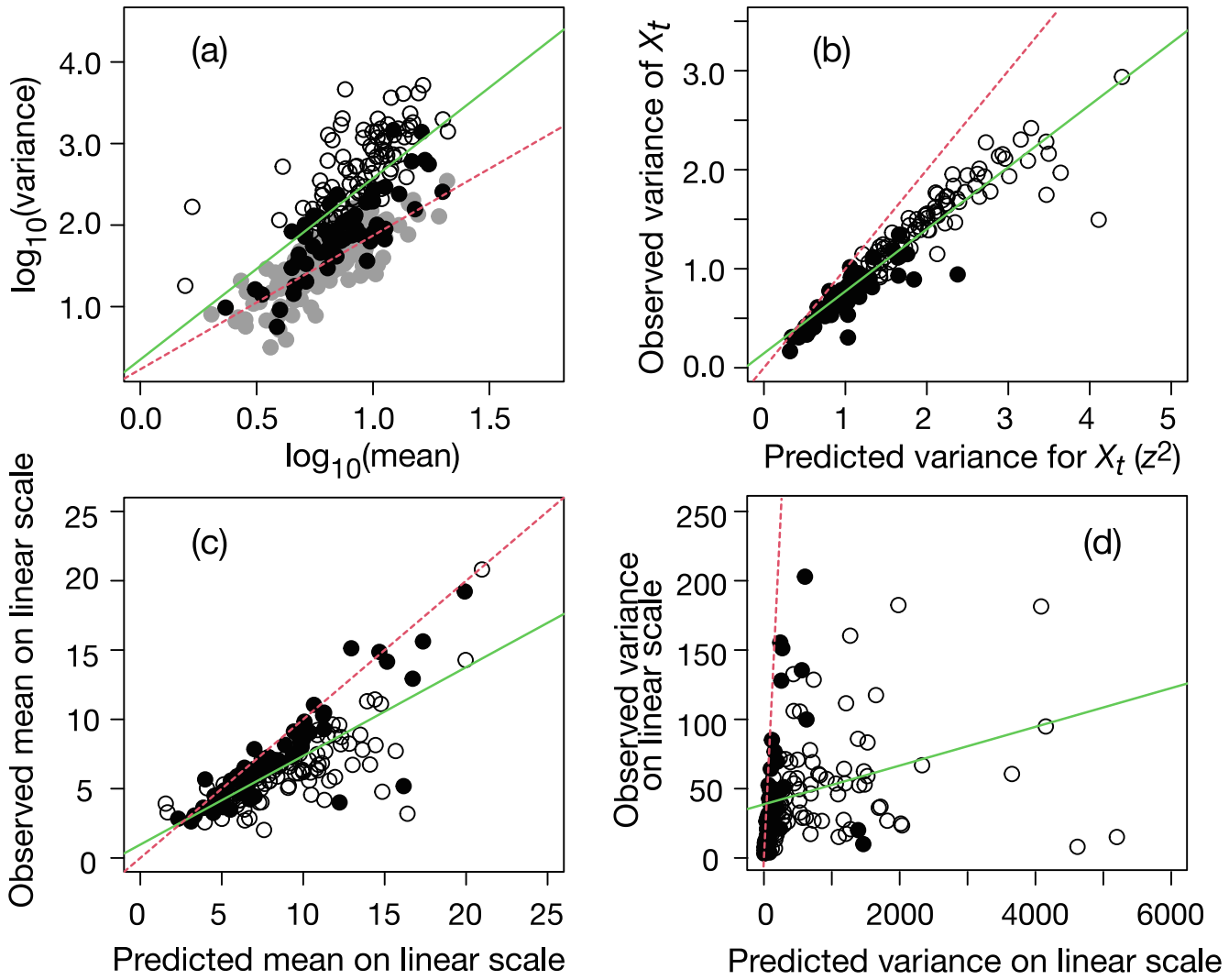

FIGURE 7 Comparisons between the observed and predicted Taylor's law (TL) characteristics from 154 populations. The predicted values were calculated using the parameters of the second-order autoregressive model (see Equations 3–5 in the main text). Eight populations were excluded from analyses because their predicted variances were unrealistically extreme (predicted variance <0 from two populations and predicted variance >10,000 from six populations). Solid and open circles denote the populations with $\sigma_j \leq 1$ and $\sigma_j > 1$, respectively. For (b), (c), and (d), broken lines are the isoline ($y = x$), while solid lines represent a significant linear relationship between observed and predicted values. (a) The relationship of the predicted variance to the predicted mean of population density. Each point represents the relationship of $\log_{10}(\mathrm{Var}(N_{t,j}))$ to $\log_{10}(E(N_{t,j}))$. Observed populations are also plotted with shaded circles. A solid line represents a significant linear relationship for predicted values, while a broken line is the observed TL line. (b) The observed variances of the centered logarithmic density ($X_{t,j}$) are plotted as a function of the predicted ones (z_j^2). (c) The observed means on the linear scale are plotted as a function of the predicted ones on the linear scale. (d) The observed variances on the linear scale are plotted as a function of the predicted ones on the linear scale. The scales differ between *x*- and *y*-axes.

variances were widely scattered under the isoline, although the relationship between the predicted and observed variances was statistically supported ([observed variance$_j$] $= 38.697 + 0.014 \times$ [predicted variance$_j$], $t = 3.467$, $p = 0.0007$, $R^2 = 0.067$, Figure 7d, and the 95% confidence interval of the slope 0.014 was 0.006–0.022).

The deviation of the predicted mean$_j$ and variance$_j$ from the observed ones consistently depended on σ_j^2 but not density-dependent coefficients (Table S7). Larger deviations in predicted mean$_j$ were found in populations with larger σ_j^2, and predicted variance$_j$ also showed larger deviations from the observed variance$_j$ in populations with higher σ_j^2.

The predicted variance of $X_{t,j}$ by Equation (3) (z_j^2) ranged from 0.320 to 4.396. It can be proved that the difference between z_j^2 and $\ln(\exp(z_j^2) - 1)$ must be less than 0.145 when $z_j^2 \geq 2$, and this relationship was empirically confirmed (Figure S6). The model (Equation 7) exhibited

an excellent performance (Figure S7): $\log_{10}(\mathrm{Var}(N_{t,j})) = -0.371 + 2.036 \times \log_{10}(E(N_{t,j})) + 0.555 \times z_j^2$ ($F = 7648$, $p < 2 \times 10^{-16}$, Adjusted $R^2 = 0.990$). The coefficient 2.036 of $\log_{10}(E(N_{t,j}))$ (SE = 0.026, with 95% confidence interval 1.984–2.088) was close to and included the theoretical prediction (2.0), and the coefficient 0.555 for z_j^2 (SE = 0.006, with 95% confidence interval 0.542–0.567) was also not far from the predicted value (1/2.3 = 0.435). The highly accurate performance of the model using $\ln(\exp(z_j^2) - 1)$ instead of z_j^2 was confirmed: $\log_{10}(\mathrm{Var}(N_{t,j})) = 1.3 \times 10^{-15} + 2.0 \times \log_{10}(E(N_{t,j})) + 0.434 \times \ln(\exp(z_j^2) - 1)$ (Adjusted $R^2 \approx 1$).

4 | DISCUSSION

Taylor's law describes one relationship between the variance and mean of population density for a population assembly and is usually tested by an ordinary least-squares regression method. Although some models predict that the temporal TL slope equals 2 (Ballantyne, 2005; Cohen, 2013; Kilpatrick & Ives, 2003), most observed slopes satisfy $1 < b < 2$ (Taylor & Woiwod, 1980, Linnerud et al., 2013, Cobain et al., 2019, but see Tippett & Cohen, 2016; Zhao et al., 2019). This widespread discrepancy between empirical populations and some theory can be solved by understanding how variables other than $\log_{10}$(mean) influence $\log_{10}$(variance). Many factors have been proposed as influential on TL slopes (e.g., species interaction: Kilpatrick & Ives, 2003, reproductive correlation: Ballantyne & Kerkhoff, 2007, habitat size: Mellin et al., 2010, demographic stochasticity: Linnerud et al., 2013, environmental variability: Cobain et al., 2019). Identifying influential variables should contribute to understanding how those biological factors work. Saitoh and Cohen (2018) and Cohen and Xu (2015) suggest that the density-dependent coefficients, density-independent parameters of the second-order autoregressive model and the skewness of population density can help to explain the variation of $\log_{10}$(variance) beyond the variation explained by $\log_{10}$(mean).

The 162 observed populations satisfied the temporal TL with slope $b = 1.687$ (Figure 2). The studied populations were distributed approximately 420 km from south to north and 390 km from west to east (Figure 1). The seven geographic groups varied widely in population dynamics (Figure 3) and density dependence (Figure 4 and Figure 5). The south-western populations of Group IV and Group VIII showed lower population densities and weaker density dependence for 1-year lag (higher $\alpha_{1,j}$). Although the temporal TL slopes varied between the groups ranging from 1.284 to 2.187, those slopes did not significantly differ from the overall slope ($b = 1.687$). Therefore, the TL model for the overall populations was robust. However, the proportion of the $\log_{10}(\mathrm{variance_j})$ variation explained by $\log_{10}$(mean) was moderate (0.62), suggesting that other variables than $\log_{10}$(mean) also influence $\log_{10}$(variance).

4.1 | Variables that influence the variance

Table 2 demonstrated that the density-independent parameters σ_j^2 and γ_j were particularly significantly associated with $\log_{10}(\mathrm{variance}_j)$ in addition to $\log_{10}(\mathrm{mean}_j)$. All effects of σ_j^2, γ_j, and $\log_{10}(\mathrm{mean}_j)$ were positive on $\log_{10}(\mathrm{variance}_j)$. If $\log_{10}(\mathrm{mean}_j)$ is not associated with σ_j^2 and γ_j, then $\log_{10}(\mathrm{variance}_j)$ would increase with the increase of $\log_{10}(\mathrm{mean}_j)$ along the null expectation for the temporal TL slope = 2. To realize the empirically observed slope ($b < 2$), the increase of $\log_{10}(\mathrm{variance}_j)$ should slow as $\log_{10}(\mathrm{mean}_j)$ increases. The negative relationships between σ_j^2 and $\log_{10}(\mathrm{mean}_j)$ and between γ_j and $\log_{10}(\mathrm{mean}_j)$ in the studied populations (Figure S5) worked as the mechanism that reduced the increase of $\log_{10}(\mathrm{variance}_j)$ with the increase of $\log_{10}(\mathrm{mean}_j)$.

The density-dependent effects for 2-year lag ($\alpha_{2,j}$) negatively affected $\log_{10}(\mathrm{variance}_j)$ and could regulate the effect of $\log_{10}(\mathrm{mean}_j)$ on $\log_{10}(\mathrm{variance}_j)$. However, the magnitude of $\alpha_{2,j}$ effects was inferior to that of σ_j^2 and γ_j. Another density-dependent effect ($\alpha_{1,j}$) had minor influence on $\log_{10}(\mathrm{variance}_j)$.

A limitation of this study is that several of our statistical comparisons should be interpreted descriptively rather than probabilistically when the data violate the assumptions of these tests. For example, the Kruskal–Wallis rank sum test, a one-way analysis of variance based on ranks, assumes that all observations are independent within and among samples. Because of synchrony among some of the vole populations, the assumption that all observations are independent does not always hold. In the absence of independent observations, a low p-value must be interpreted as a descriptive indicator that some populations have higher densities (or other statistics) than other populations, rather than as a probabilistically precise statement. The Dwass–Steel–Critchlow–Fligner test, which is used after the Kruskal–Wallis test gives a "significant" result, is subject to the same caveats.

Another limitation of our statistical analysis is that OLS regression of log variance as a function of log mean assumes that the values of log mean are known without error, whereas in fact both log mean and log variance are subject to sampling variation. However, the sampling variation of log mean is likely to be very much less than

the sampling variation of log variance. The resulting bias in estimating the slope b is likely to be small. Visual inspection of the data points and regression lines supports the conclusion that OLS regression of the log moments gives reasonable, if not statistically optimal, results.

4.2 | Variability and skewness

The parameter σ_j^2 represents the amount of variation of population density that the Gompertz model could not capture. It is derived from various sources that can push population density away from the mean density, which the Gompertz model interprets as an equilibrium density. The potential sources include environmental variability, density-independent interactions in a population, genetic drift of local populations leading to phenotypic variation in responses to density and the environment, and interactions of any or all of these factors. Evolutionary effects may be minor in the studied populations because the time series lasted only 23–31 years. Among ecological effects, three forms of stochasticity are widely held to influence population dynamics: demographic, environmental, and catastrophic effects (Lande, 1993). Demographic stochasticity is relevant to only very small populations, and catastrophic events are rare. Therefore, environmental variability may be the primary source of σ_j^2 for the studied populations. Sæther et al. (2016) suggest that population dynamics with small population sizes are primarily influenced by environment-driven variation in recruitment, whereas close to the carrying capacity, variation in population growth is more strongly influenced by density-dependent mortality. This mechanism can explain the negative relationship between σ_j^2 and $\log_{10}(\text{mean}_j)$.

The frequency distribution of overall population densities was approximated by a negative binomial distribution (Figure 6a). The most frequent (modal) density class was the lowest bin of the histogram, and the distribution was highly right-skewed. The geographic groups with higher densities than the overall average (Group I, II, and V) showed lower skewness. However, a population with a high mean density did not always show a lower skewness. The populations of Group IV and VIII with low mean densities showed lower skewness. Although the skewness decreased with the increase in mean density in general, this pattern may depend on the situation.

Taylor (1984) observed that insect populations at progressively higher densities conformed to different frequency distributions (e.g., Poisson, negative binomial, and lognormal) with identical slope b. Cohen and Xu (2015) verify that the TL slope can be predicted from the sample skewness and the sample coefficient of variation of population density under the assumption of independent and identically distributed observations. Although the studied populations did not satisfy this assumption, the skewness (γ_j) significantly influenced the variation of $\log_{10}(\text{variance}_j)$, and the negative correlation of γ_j and $\log_{10}(\text{mean}_j)$ might be critical in determining the TL slope b. Another approach independent of Cohen and Xu (2015) is necessary to understand the effect of skewness on the variance of population density observed in this study.

Cohen (2020) showed that, as a result of rescaling and translation, any family of frequency distributions of population densities with positive means and positive variances can be made to obey TL or any other relation of variance to mean in a metapopulation or other collection of populations (see also Mallmin, 2022). However, there is still little empirical information about how actual density distributions are associated with the TL slope b. Future studies should examine further the associations between population dynamics and the frequency distribution of population density and the mean–variance relationship of the frequency distribution.

4.3 | Null and empirical slopes

Equation (7) tells us that the mean population density alone cannot explain the variation of density variance and that the potential coefficient of the mean population density is two, which is the null value of the TL slope. This study validated Equation (7) using the empirical data. The coefficient of the mean density (1.949) was close to the null value in the model of Table 2, which explained the great majority of the variation of population density variance (Adjusted $R^2 = 0.939$). When removing other explanatory variables than the mean density, leaving only TL, the coefficient of $\log_{10}(\text{mean})$ = the TL slope (1.687) was below the null value, and the goodness of fit of the model decreased (Adjusted $R^2 = 0.620$). If these relationships hold beyond the single example studied here, when the effects of the variables listed in Table 2 were significant, the TL slope b would be below two.

Most predicted values based on Equations (3)–(5) were higher than the observed values, and higher variances of population density may have caused the steeper TL slope in the predicted values (Figure 7). Those predictions require the lognormal distribution of population density and a long length of time series for an asymptotic value. These requirements were not satisfied in reality. The log–log survival plot showed that the population densities of the studied populations diverged from the

lognormal distribution (Figure S4), and the lengths of time series were limited (23–31 years). The deviation of the predicted values from the observed ones was evident in populations with $\sigma_j > 1$. Five of six populations of which variances were unrealistically high (>10,000) showed high σ_j ranging from 1.676 to 2.042, and σ_j of the remaining one was 0.997. Since σ_j is squared in the process of the variance prediction, the discrepancy between observed and predicted variances may be escalated by $\sigma_j > 1$. In addition, unrealistic predicted variances came from the time series with a shorter length (two from 27 years and six from 23 years). These results suggest that the observed σ_j may be overestimated by the short length of the time series, or the second-order autoregressive model may not sufficiently capture the characteristics of the population dynamics of the studied populations. We should improve parameter estimation techniques and population dynamics models.

To understand the empirical results in Table 2 theoretically, we combine Equations (3) and (7). This combination expresses $\log_{10}(\text{variance}_j)$ in terms of $\log_{10}(\text{mean}_j)$ and the parameters of the Gompertz model, for all populations j, asymptotically for large time t and asymptotically for large z_j^2

$$\log_{10}\left(\text{Var}\left(N_{t,j}\right)\right) = 2\times\log_{10}\left(E\left(N_{t,j}\right)\right) + \frac{1}{2.3}\times\frac{1-\alpha_{2,j}}{1+\alpha_{2,j}} \times\frac{\sigma_j^2}{\left(1-\alpha_{2,j}\right)^2-\left(1+\alpha_{1,j}\right)^2}.$$

From the first term on the right, $2\times\log_{10}\left(E\left(N_{t,j}\right)\right)$, it is obvious that $\log_{10}(\text{variance}_j)$ should be proportional to two times $\log_{10}(\text{mean}_j)$, when all else is held constant. Table 2 gives the linear coefficient of $\log_{10}(\text{mean}_j)$ as 1.949.

In the second term on the right are the three Gompertz parameters. For qualitative analysis, we approximated $\alpha_{1,j} \approx -1$, because the observed $\alpha_{1,j}$ was around -1 in most populations. When $\alpha_{1,j}$ -1, it disappears from the expression for z_j^2 and from the second term on the right. Thus, in Table 2, we expect the small coefficient and insignificant role of $\alpha_{1,j}$. With this approximation, the second term on the right becomes

$$\frac{1}{2.3}\times\frac{1-\alpha_{2,j}}{1+\alpha_{2,j}}\times\frac{\sigma_j^2}{\left(1-\alpha_{2,j}\right)^2-\left(1+\alpha_{1,j}\right)^2} \approx \frac{1}{2.3}\times\frac{1-\alpha_{2,j}}{1+\alpha_{2,j}} \times\frac{\sigma_j^2}{\left(1-\alpha_{2,j}\right)^2} = \frac{1}{2.3}\times\frac{\sigma_j^2}{1-\alpha_{2,j}^2}.$$

Furthermore, assuming $\alpha_{2,j}$ is constant at the average (-0.149), the second term can be simplified as follows:

$$\log_{10}\left(\text{Var}\left(N_{t,j}\right)\right) = 2\times\log_{10}\left(E\left(N_{t,j}\right)\right) + 0.445\times\sigma_j^2.$$

The empirical model ($\log_{10}(\text{variance}_j)$ $\log_{10}(\text{mean}_j)$ $+ \sigma_j{}^2$) gave the coefficients of $\log_{10}(\text{mean}_j)$ and σ_j^2 as 1.830 and 0.213, respectively.

As $\alpha_{2,j}^2$ increases from 0 to 1, the denominator $1-\alpha_{2,j}^2$ decreases from 1 to 0 so the ratio $\sigma_j^2/\left(1-\alpha_{2,j}^2\right)$ increases from σ_j^2 to infinity. Figure S3B shows that a majority of values of $\alpha_{2,j}$ are between -1 and 0. As $\alpha_{2,j}$ increases from -1 to 0, the ratio $\sigma_j^2/\left(1-\alpha_{2,j}^2\right)$ decreases. Since the decreasing effect on $\sigma_j^2/\left(1-\alpha_{2,j}^2\right)$ as $\alpha_{2,j}$ increases from -1 to 0 dominates the increasing effect on $\sigma_j^2/\left(1-\alpha_{2,j}^2\right)$ as $\alpha_{2,j}$ increases from 0 to 1, the positive effect of $\sigma_j{}^2$ on $\log_{10}(\text{variance}_j)$ is reduced by the increase of $\alpha_{2,j}$. Therefore, the negative coefficient of $\alpha_{2,j}$ in Table 2 can be theoretically interpreted.

The effect of skewness on $\log_{10}(\text{variance}_j)$ can be also qualitatively explained. When $N_{t,j}$ is lognormally distributed, the skewness of $N_{t,j}$ is given as $\varepsilon_j = \left(\exp\left(z_j^2\right)+2\right)\left(\exp\left(z_j^2\right)-1\right)^{1/2}$. Therefore, the skewness is included into Equation (6) by replacing the term of $\exp(z_j{}^2)$ –1 of Equation (6) with a term containing ε_t: $\exp\left(z_j^2\right)-1 = \frac{\varepsilon_j^2}{\left(\exp\left(z_j^2\right)+2\right)^2}$.

$$\ln\left(\text{Var}\left(N_{t,j}\right)\right) = 2\times\ln\left(E\left(N_{t,j}\right)\right) + \ln\left(\frac{\varepsilon_j^2}{\left(\exp\left(z_j^2\right)+2\right)^2}\right) = 2\times\ln\left(E\left(N_{t,j}\right)\right) + 2\times\ln\left(\varepsilon_j\right) - 2\times\ln\left(\exp\left(z_j^2\right)+2\right),$$

$$\log_{10}\left(\text{Var}\left(N_{t,j}\right)\right) = 2\times\log_{10}\left(E\left(N_{t,j}\right)\right) + 2\times\log_{10}\left(\varepsilon_j\right) - 2\times\log_{10}\left(\exp\left(z_j^2\right)+2\right).$$

The accurate performance of this model was confirmed using the parameter estimates of the 162 vole populations: $\log_{10}(\text{Var}(N_{t,j})) = 2.7\times10^{-16} + 2.0\times\log_{10}(E(N_{t,j})) + 2.0\times\varepsilon_j - 2.0\times\log_{10}(\exp(z_j{}^2)+2)$ ($F = 4.1\times10^{31}$, $p < 2\times10^{-16}$, Adjusted $R^2 \approx 1$), but Table 2 gave the coefficient of γ_j as 0.182 instead of 2 for ε_t.

The linear model used in Table 2 is a crude approximation to the real relationship that is nonlinear, and the exact agreement between theoretical and empirical coefficients is not expected. However, as discussed above, the effects of the parameters of the Gompertz model and

the skewness of population density on the density variance, which were empirically demonstrated, can be theoretically interpreted.

AUTHOR CONTRIBUTIONS

Takashi Saitoh conceived the ideas of this study and analyzed the data; Joel E. Cohen developed theoretical modeling. Both authors contributed critically to the manuscript and gave final approval for publication.

ACKNOWLEDGMENTS

Hayato Iijima helped Takashi Saitoh to model the dynamics of populations. Roseanne Benjamin assisted Joel E. Cohen during this work. The manuscript was greatly improved by the suggestions and comments from the reviewers (Nigel G. Yoccoz and anonymous).

CONFLICT OF INTEREST STATEMENT

The authors declare no conflicts of interest.

ORCID

Takashi Saitoh https://orcid.org/0000-0003-4085-5014
Joel E. Cohen https://orcid.org/0000-0002-9746-6725

REFERENCES

Anderson, R. M., Gordon, D. M., Crawley, M. J., & Hassel, M. P. (1982). Variability in the abundance of animal and plant species. *Nature*, *296*(5854), 245–248. https://doi.org/10.1038/296245a0

Ballantyne, F. I. (2005). The upper limit for the exponent of Taylor's power law is a consequence of deterministic population growth. *Evolutionary Ecology Research*, *7*(8), 1213–1220.

Ballantyne, F. I., & Kerkhoff, A. J. (2007). The observed range for temporal mean-variance scaling exponents can be explained by reproductive correlation. *Oikos*, *116*(1), 174–180. https://doi.org/10.1111/j.2006.0030-1299.15383.x

Box, G. E. P., & Jenkins, G. (1970). *Time series analysis and control*. Holden-Day.

Cobain, M. R. D., Brede, M., & Trueman, C. N. (2019). Taylor's power law captures the effects of environmental variability on community structure: An example from fishes in the North Sea. *Journal of Animal Ecology*, *88*(2), 290–301. https://doi.org/10.1111/1365-2656.12923

Cohen, J. E. (2013). Taylor's power law of fluctuation scaling and the growth-rate theorem. *Theoretical Population Biology*, *88*, 94–100. https://doi.org/10.1016/j.tpb.2013.04.002

Cohen, J. E. (2020). Every variance function, including Taylor's power law of fluctuation scaling, can be produced by any location-scale family of distributions with positive mean and variance. *Theoretical Ecology*, *13*, 1–5. https://doi.org/10.1007/s12080-019-00445-7 correction 2022 Theoretical Ecology, *15*, 93–94.

Cohen, J. E., Davis, R. A., & Samorodnitsky, G. (2022). COVID-19 cases and deaths in the United States follow Taylor's law for heavy-tailed distributions with infinite variance. *Proceedings of the National Academy of Sciences*, *119*(38), e2209234119. https://doi.org/10.1073/pnas.2209234119

Cohen, J. E., & Saitoh, T. (2016). Population dynamics, synchrony, and environmental quality of Hokkaido voles lead to temporal and spatial Taylor's laws. *Ecology*, *97*(12), 3402–3413. https://doi.org/10.1002/ecy.1575

Cohen, J. E., & Xu, M. (2015). Random sampling of skewed distributions implies Taylor's power law of fluctuation scaling. *Proceedings of the National Academy of Sciences of the United States of America*, *112*(25), 7749–7754. https://doi.org/10.1073/pnas.1503824112

Döring, T. F., Knapp, S., & Cohen, J. E. (2015). Taylor's power law and the stability of crop yields. *Field Crops Research*, *183*, 294–302. https://doi.org/10.1016/j.fcr.2015.08.005

Gelman, A. (2006). Prior distributions for variance parameters in hierarchical models (comment on article by Browne and Draper). *Bayesian Analysis*, *1*(3), 515–534. https://doi.org/10.1214/06-ba117a

Kaneko, Y., Nakata, K., Saitoh, T., Stenseth, N. C., & Bjornstad, O. N. (1998). The biology of the vole *Clethrionomys rufocanus*: A review. *Researches on Population Ecology*, *40*(1), 21–37. https://doi.org/10.1007/bf02765219

Kilpatrick, A. M., & Ives, A. R. (2003). Species interactions can explain Taylor's power law for ecological time series. *Nature*, *422*, 65–68. https://doi.org/10.1038/nature01471

Lande, R. (1993). Risks of population extinction from demographic and environmental stochasticity and random catastrophes. *The American Naturalist*, *142*(6), 911–927. https://doi.org/10.1086/285580

Linnerud, M., Sæther, B., Grøtan, V., Engen, S., Noble, D. G., & Freckleton, R. P. (2013). Interspecific differences in stochastic population dynamics explains variation in Taylor's temporal power law. *Oikos*, *122*(8), 1207–1216. https://doi.org/10.1111/j.1600-0706.2012.20517.x

Mallmin, E. (2022). Comments on: "Every variance function ... can be produced by any location-scale family...". *Theoretical Ecology*, *15*(4), 283–284. https://doi.org/10.1007/s12080-022-00547-9

Mellin, C., Huchery, C., Caley, M. J., Meekan, M. G., & Bradshaw, C. J. A. (2010). Reef size and isolation determine the temporal stability of coral reef fish populations. *Ecology*, *91*(11), 3138–3145. https://doi.org/10.1890/10-0267.1

Meyer, D., Dimitriadou, E., Hornik, E., Weingessel, A., Leisch, F., Chang, C.-C., & Lin, C.-C. (2022). package 'e1071' 1.7-12. https://CRAN.R-project.org/package=e1071

Pertoldi, C., Bach, L. A., & Loeschcke, V. (2008). On the brink between extinction and persistence. *Biology Direct*, *3*(1), 47. https://doi.org/10.1186/1745-6150-3-47

R Core Team. (2022). *R: A language and environment for statistical computing*. R Foundation for Statistical Computing https://www.R-project.org/

Reed, D. H., & Hobbs, G. R. (2004). The relationship between population size and temporal variability in population size. *Animal Conservation*, *7*(1), 1–8. https://doi.org/10.1017/s1367943004003476

Sæther, B.-E., Grøtan, V., Engen, S., Coulson, T., Grant, P. R., Visser, M. E., Brommer, J. E., Grant, R., Gustafsson, L., Hatchwell, B. J., Jerstad, K., Karell, P., Pietinäinen, H., Roulin, A., Røstad, O. W., & Weimerskirch, H. (2016). Demographic routes to variability and regulation in bird populations. *Nature Communications*, *7*, 1–8. https://doi.org/10.1038/ncomms12001

Saitoh, T. (2020). Effects of environmental synchrony and density-dependent dispersal on temporal and spatial slopes of Taylor's law. *Population Ecology*, *62*(3), 300–316. https://doi.org/10.1002/1438-390x.12051

Saitoh, T., & Cohen, J. E. (2018). Environmental variability and density dependence in the temporal Taylor's law. *Ecological Modelling*, *387*, 134–143. https://doi.org/10.1016/j.ecolmodel.2018.07.017

Saitoh, T., Stenseth, N. C., & Bjornstad, O. N. (1997). Density dependence in fluctuating grey-sided vole populations. *Journal of Animal Ecology*, *66*(1), 14. https://doi.org/10.2307/5960

Saitoh, T., Stenseth, N. C., & Bjørnstad, O. N. (1998). The population dynamics of the vole *Clethrionomys rufocanus* in Hokkaido, Japan. *Researches on Population Ecology*, *40*(1), 61–76. https://doi.org/10.1007/BF02765222

Stan Development Team. (2022). RStan: The R interface to Stan. R package version 2.21.7. https://mc-stan.org/

Stenseth, N. C., Bjørnstad, O. N., & Falck, W. (1996). Is spacing behaviour coupled with predation causing the microtine density cycle? A synthesis of current process-oriented and pattern-oriented studies. *Proceedings of the Royal Society of London. Series B: Biological Sciences*, *263*(1376), 1423–1435. https://doi.org/10.1098/rspb.1996.0208

Stenseth, N. C., Bjornstad, O. N., & Saitoh, T. (1996). A gradient from stable to cyclic populations of Clethrionomys rufocanus in Hokkaido, Japan. *Proceedings of the Royal Society of London. Series B: Biological Sciences*, *263*(1374), 1117–1126. https://doi.org/10.1098/rspb.1996.0164

Stenseth, N. C., Bjørnstad, O. N., & Saitoh, T. (1998). Seasonal forcing on the dynamics of *Clethrionomys rufocanus*: Modeling geographic gradients in population dynamics. *Researches on Population Ecology*, *40*, 85–95. https://doi.org/10.1007/bf02765224

Stenseth, N. C., Viljugrein, H., Saitoh, T., Hansen, T. F., Kittilsen, M. O., Bølviken, E., & Glöckner, F. (2003). Seasonality, density dependence, and population cycles in Hokkaido voles. *Proceedings of the National Academy of Sciences of the United States of America*, *100*(20), 11478–11483. https://doi.org/10.2307/3147817?ref=search-gateway:db87af07ac2a9ce9b811f771a3acc438

Tatewaki, M. (1958). Forest ecology of the islands of the north Pacific Ocean. *Journal of the Faculty of Agriculture, Hokkaido University*, *50*, 371–486. http://hdl.handle.net/2115/44083

Taylor, L. R. (1961). Aggregation, variance and the mean. *Nature*, *189*, 732–735. https://doi.org/10.1038/189732a0

Taylor, L. R. (1984). Assessing and interpreting the spatial distributions of insect populations. *Annual Review of Entomology*, *29*, 321–357. https://doi.org/10.1146/annurev.ento.29.1.321

Taylor, L. R. (1986). Synoptic dynamics, migration and the Rothamsted insect survey—Presidential-address to the British-Ecological-Society, December 1984. *Journal of Animal Ecology*, *55*(1), 1–38. https://doi.org/10.2307/4690

Taylor, L. R., & Woiwod, I. P. (1980). Temporal stability as a density-dependent species characteristic. *Journal of Animal Ecology*, *49*(1), 209–224. https://doi.org/10.2307/4285

Taylor, R. A. J. (2019). *Taylor's power law: Order and pattern in nature*. Elsevier Academic Press.

Tippett, M. K., & Cohen, J. E. (2016). Tornado outbreak variability follows Taylor's power law of fluctuation scaling and increases dramatically with severity. *Nature Communications*, *7*(1), 10668. https://doi.org/10.1038/ncomms10668

Zhao, L., Sheppard, L. W., Reid, P. C., Walter, J. A., & Reuman, D. C. (2019). Proximate determinants of Taylor's law slopes. *Journal of Animal Ecology*, *88*(3), 484–494. https://doi.org/10.1111/1365-2656.12931

SUPPORTING INFORMATION

Additional supporting information can be found online in the Supporting Information section at the end of this article.

How to cite this article: Saitoh, T., & Cohen, J. E. (2024). Quantifying factors that explain the slopes of the temporal Taylor's law of Hokkaido vole populations. *Population Ecology*, *66*(3), 125–142. https://doi.org/10.1002/1438-390X.12176